Model-dependent small-angle scattering for the study of complex organic materials

Andrew R. McCluskey[ab] and Karen J. Edler[a*]

[a]*Department of Chemistry, University of Bath, Claverton Down, Bath, UK*
[b]*Diamond Light Source, Diamond House, Rutherford Appleton Laboratory, Harwell-Oxford, UK*

Abstract: Small-angle scattering (SAS) is a powerful technique capable of determining the sample averaged structure of systems within size ranges of 1 nm to ~500 nm. This is particularly useful when applied to the study of self-assembled organic systems, which are often in this size range. SAS is an umbrella term to describe both small-angle X-ray scattering (SAXS) and small-angle neutron scattering (SANS); within this review both techniques will be discussed with a focus on the analysis of the experimental data and the systems to which these techniques can be applied. A series of applications are also discussed; the ambition is that this will give an appreciation of the possible utilities of these techniques.

Keywords: SAXS, SANS, peptides, polymers, micelles, surfactants, scattering, analysis, model-dependent.

The importance of the synthesis of molecular components, designed as constituents in ordered molecular assemblies, means that interest in the characterization of such nanoscopic aggregates in solution has grown among synthetic chemists. [1-3] Small angle scattering is a powerful technique for study of small aggregates in solution, with straightforward sample preparation and without the need for staining or drying of the sample. Thus it is particularly suited to solution investigations of self-assembled organic constructs. This review aims to give a summary of the capabilities these techniques and the analysis of small angle scattering data, as well as some recent examples where SAS has been used for characterization of such systems. If this brief discussion sparks further interest, the theory and practice of small angle scattering is covered in much greater detail in many well-recognised texts. [4-6]

1. THEORY OF SCATTERING

Due to the development of user-friendly software to aid in the analysis of SAS experiments, such as SASView [7] and SASfit, [8] an in-depth knowledge of scattering theory is no longer a pre-requisite to the analysis of SAS profiles. However, in order to ensure that analysis is carried out without bias or error it is important to have some level of foundation knowledge.

1.1. Scattering vector

SAS involves the scattering of some probing radiation by the sample. SAS is an elastic scattering technique, like traditional crystallography, in that the energy of the probing radiation does not change during the scattering event. The direction and magnitude of the probing and scattering radiation can be described by a pair of wavevectors, $\mathbf{k}_\mathrm{i}$ and $\mathbf{k}_\mathrm{f}$. It is the difference between the incident and final wavevectors that gives rise to the scattering vector, $\mathbf{Q}$, where,

$$\mathbf{Q} = \mathbf{k}_\mathrm{i} - \mathbf{k}_f.$$

The scattering vector and wavevectors, as reciprocal distances, have the SI unit of m^{-1}. However, due to the length-scales being probed it is often more convenient to use units of nm^{-1} or $Å^{-1}$. In the elastic scattering vector, the wavelength, λ, of the radiation will not change, and as a result the magnitude of the scattering vectors are the same and can be found as follows,

$$|\mathbf{k_i}| = |\mathbf{k_f}| = \frac{2\pi}{\lambda}$$

and hence it is only the direction of the vector that is changing. This means that it is possible to apply simple trigonometry to this scattering and determine the relation of the magnitude of the scattering vector, $Q = |\mathbf{Q}|$, to the angle of scattering, 2θ, and radiation wavelength, λ. Using the vector diagram shown in Figure 1, it can be seen that $Q/2$ can be found as,

$$\frac{Q}{2} = |\mathbf{k}_i| \sin\theta$$

Then by combining the above two equations it can be shown that,

$$Q = \frac{4\pi \sin\theta}{\lambda}$$

For an isotropic scattering pattern, e.g. 1-dimensional, it is the magnitude of the scattering vector that is measured. Practically, the evaluation of Q creates a radiation independent measurement as, despite there being no energy

*Department of Chemistry, University of Bath, Bath, UK, BA2 7AY, Email: k.edler@bath.ac.uk

change during scattering, the energy of the radiation will affect the angle through which the wavevector scatters.

1.2. Experimental considerations

While the focus of this review will be on the analysis of SAS patterns, it is necessary to also consider a few experimental aspects. This is where it is important to consider the differences between X-rays and neutrons.

X-rays are a form of electromagnetic radiation which interact with the electrons in a system. The generation of X-ray beams is feasible both in laboratories and at large scale facilities such as the European Synchrotron Radiation Facility (ESRF). Common laboratory sources include X-ray tubes, rotating anodes, and the new liquid gallium sources. Laboratory suitable SAXS instruments are available commercially and are becoming increasing powerful and cost-effective. However, the X-ray brilliance available from a laboratory source is dwarfed by the large scale synchrotron facilities, allowing for shorter sample collection times and higher quality data as a result. Additionally, due to the high flux available at large scale facilities, quality SAXS patterns can be obtained with relatively small sample sizes, for example the BioSAXS beamline (BM29) at the ESRF requires only 30 μL of sample at concentrations of ~10 mg ml^{-1}. [9] It is however important to be aware of the adsorption of X-rays by particular atoms, and that these X-rays can be re-emitted with some energy difference, with the energy being transferred to the molecules that absorbed the radiation. This absorption mechanism is particularly common in materials rich in heavy elements, and as a result it is difficult to obtain reliable scattering patterns from such materials. Practically this means that chlorinated solvents, for instance, are unsuitable for SAXS experiments as the high adsorption masks any scattering from the sample. Additionally, this adsorption and re-emission process is one of the possible mechanisms for beam damage during SAXS data capture, where the intense brilliance of the SAXS beam is capable of altering the structure of a molecule. Therefore, it is important to ensure that any structural change in time-resolved SAXS can be attributed to deliberate efforts rather than beam damage.

In comparison with X-rays the quantity of sample required for a small-angle neutron scattering experiment is significantly larger, usually in the region of 0.5 ml of solution. This is due to the very weak interaction that the neutron has with other materials. Additionally, unlike X-rays it is not possible to produce neutrons on a laboratory scale and as a result it is necessary to visit a large scale neutron facility such as ISIS at the Rutherford Appleton Laboratory, UK or the Institut Laue-Langevin, in France. A major experimental consideration in the use of SANS is the presence of incoherent scattering which gives rise to the background of a scattering pattern. While this is low for many atoms commonly found in organic molecules, the incoherent scattering for hydrogen is very high. This means that a highly hydrogenous sample will have a significant background associated with it, often masking features of the scattering. However, this may be overcome with the use of deuterium in place of hydrogen, this is also important in terms of the contrast-matching effect discussed below.

1.3. Contrast

Small angle scattering is used to probe structure of objects with size larger than 1 nm, so that the structures probed are assemblies of atoms, rather than the inter-atomic distances measured in crystallographic techniques. The shape of the SAS pattern observed is dependent on three factors:

- the spatial arrangement of the objects in the system,
- the instrument that is being used to measure the pattern, and
- the interaction between the radiation and the matter under investigation.

This final factor is often referred to as the scattering length, b. Since small angle scattering probes nanoscopic clusters of atoms, both the scattering length of the atoms, and their local arrangement in space (i.e. density) are important. This is quantified in the scattering length density (ρ), which is a property of the molecules present in a material, defined as:

$$\rho = \frac{N_A d}{M_W} \sum_i b_i$$

where N_A is Avogadro's number, M_W is the molecular mass of the species in the aggregate, d is the physical density of the material and b is the scattering length of all of the atoms present in the aggregate. The scattering length density (SLD) of an aggregate can be calculated from the mole fraction of each molecular component in that object. Scattering is observed from an interface where the scattering length density changes e.g. between a particle and the solvent in which it is suspended. Many online SLD calculators exist, such as that developed by the NIST Center for Neutron Research (https://www.ncnr.nist.gov/resources/activation/), these are often the starting point in the planning of a SAS experiment. For less well defined macromolecular species, or species which may undergo hydrogen exchange in deuterated solvents such as proteins, it is often necessary to determine the SLD experimentally.

The scattering of an X-ray by a particle is due to the interaction between the X-ray and the electron cloud of the atoms within the particle. This leads to the scattering length of an atom being directly related to the number of electrons, where the scattering of a single electron is the Compton classical electron radius, [10]

$$r_e = e^2/(m_e c^2) = 2.818\times10^{-15} \text{ m}.$$

The scattering of neutrons however is due to interactions between the neutron and the nucleus of an atom so varies in a non-systematic fashion with respect to atomic number. The fact that the scattering varies with atomic mass leads to an important technique in the study of organic species, known as contrast variation. This is based on the substitution of one isotope of an atom for another, such as hydrogen ($b = -3.74$ fm) and deuterium ($b = 6.67$ fm), which does not generally introduce a change in the material properties. This technique allows for the ability to 'contrast-match' different

parts of the system to the solvent by matching the scattering length densities, and therefore reduce the dimensionality of the analysis. For example, by matching the solvent scattering length density to that of the tails of some surfactant molecules at the centre of a micelle, there would only be scattering from the heads (Figure 2b), and conversely there would only be scattering from the tails if the solvent had the same scattering length density as the head groups (Figure 2c). This means that the problem becomes more defined as the same model must fit both data sets, varying only the scattering length densities in the head or tail regions of the micelle.

There is also the possibility of using contrast variation when using X-rays, through anomalous scattering. This occurs where different wavelengths of radiation give different scattering, when the wavelengths are on opposite side on an X-ray absorption edge. This is not frequently utilised for organic materials as the X-ray absorption edges for elements commonly found in organic species (H, C, N, O, etc.) are at very low X-ray energies, and generally outside of the accessible range. [11]

2. ANALYSIS

Scattering is a reciprocal space technique, and can considered as the Fourier transform of the electron or nuclear density, for X-rays and neutrons respectively. While diffraction gives atomistic information with high angle scattering, small angle scattering gives micro- and nano-scale information. SAS however shares the loss of phase information seen in traditional crystallography. Since the scattered intensity is proportional to the square of the difference in SLD between, for instance, particle and solution, only the magnitude of the difference is retained in the measured intensity, and it cannot be determined directly whether that difference is positive or negative. Thus, without other information, it cannot be determined whether the particle has a higher SLD than the solvent or vice versa as the scattered intensity will be identical.

The SAS pattern can be thought of as consisting of two sections, which arise from the particle of the scattering species and the interactions between those particles. The form factor arises from the average shape of the scattering species, while the structure factor is a measure of the interactions between each of the scattering objects through the solvent (Figure 3). Due to the structure factor being the result of interactions between scattering particles it is often possible to control its presence by changing the sample concentration. Eventually, the concentration will be so low that there will be effectively no interaction between the scattering particles. [12] This may not be feasible if the size and shape of the scattering particle changes with concentration. For example, in a micellar system of ionic surfactants the critical micelle concentration may be higher than the minimum concentration for a structure factor to be present. [13]

The majority of SAS analysis involves the use of model-dependent methods, where parameter constraints are used to overcome the phase problem inherent in reciprocal space techniques. However, it is possible to rationalize the appearance of a SAS profile without *a priori* information through the work of Glatter and co-workers, this is discussed in great detail in reference [14]. The scattering pattern can be transformed directly into a real-space density distribution through an inverse Fourier transform procedure. This distribution can give information about the maximum particle size, and average radius of gyration. However, this method is often mathematically cumbersome and gives less information about the system under study when compared to model-dependent methods, despite the fact that the model-dependent methods rely on assumptions about the system. These assumptions can, and should, be educated, incorporating other information that is already known about the system.

2.1. Basic analysis

There are two common, straight-forward techniques that can be used to give an initial understanding of the size and shape of the scatterer. The first is the Guinier approximation, this allows for the determination of the radius of gyration, R_g, of the scattering species. [15] This scattering law is only valid at very small values of Q, where $Q < {R_g}^{-1}$, [16] and as a result it is only valid for dilute solutions so that only the form factor is present in the scattering. The Guinier law states,

$$\ln[I(Q)] = \ln[I(0)] - \left(\frac{{R_g}^2}{3}\right) Q^2,$$

where $I(Q)$ is the intensity of scattering at a given scattering vector. The radius of gyration of the scattering object can be found by graphing the scattering profile with axes $\ln[I(Q)]$ vs. Q^2, and evaluating the gradient at low Q, as is shown in Figure 4. The Guinier analysis is common-place in the study of proteins by SAS, as this allows for the determination of the protein radius R,

$$R^2 = \left(\frac{5}{3}\right) {R_g}^2,$$

in the native solution state, by assuming that it is spherical. [17]

Porod's Law allows for the quantification of the surface and therefore shape the scattering species. [18] This law is present at large values of Q, where the scattering intensity decays as,

$$I(Q) \propto SQ^{-n},$$

where S is characteristic of the surface area to volume ratio of the species, and n is associated with the shape of the species. Table 1 gives the values of n for a series of different structures. It is possible to determine the value of n by graphing, $\log[I(Q)]$ against $\log(Q)$, where the gradient is $-n$.

Table 1. Characteristic values of *n*, determined at high Q for polymeric structures.

$\boldsymbol{n}$	Structure
1	Rod
2	Disk
3-4	Rough interfaces
4	Smooth interface/Sphere

At low Q values on a $\mathbf{log}[\boldsymbol{I}(\boldsymbol{Q})]$ against $\mathbf{log}(\boldsymbol{Q})$, some evaluation of particle shape may also be possible. In this region discs and rod-shaped particles also have $\boldsymbol{n} = \mathbf{2}$, and $\mathbf{1}$ respectively but spherical particles, that are small enough to be measured within the Q range covered will give $\boldsymbol{n} = \mathbf{0}$.

2.2. Form factor

It was mentioned above that the SAS pattern consists of two parts, the form and the structure factors, both of which contribute to the scattering pattern. In the model-dependent analysis of SAS patterns, the scattering as a result of the spatial arrangement of the atoms is written as,

$$I(Q) = D\Delta\rho^2 V^2 P(Q) S(Q),$$

where, D is the number density of particles, $\Delta\rho$ is the difference in scattering length density between the particles and the solvent, V is the particle volume, $P(Q)$ is the particle form factor, and $S(Q)$ is the structure factor, for a centrosymmetric system. It is possible to use analytical or approximated approaches to understand the shape and size of the particle in solution.

The form factor is modelled using coarse shapes; such as spheres, cylinders, or ellipses. This involves the determination of analytical or quasi-analytical solutions for the scattering of the probing radiation by the shape of choice. This has been completed for a wide range of shapes, and many tables exist detailing a huge variety of calculated form factors. [19] SASfit [8] is a freely-available software which contains a large library of more than 200 different form factor solutions to aid in the model-dependent analysis of SAS patterns.

The form factor of a sphere was solved in the early 19th century by Lord Rayleigh [20]

$$P(Q) = \left\{\frac{3[\sin QR - QR\cos(QR)]}{(QR)^3}\right\}^2,$$

where R is the radius of the sphere. A comparison between a 'simulated' experimental pattern (black circles) and the scattering from the above equation is shown in Figure 5. This can be seen to have a good agreement, however the minima are not well modelled due to instrumental and polydispersity smearing.

Surfactants such as cetylpyridinium bromide (CPBr) are capable of forming long, worm-like micelles in solution, [22] which have two dimensions for which the form factor must be determined. The longitudinal part, $P_L(Q)$, and the circular cross-section, $P_{CS}(Q)$, can be combined to give the total form factor, $P(Q) = P_L(Q)P_{CS}(Q)$. The longitudinal form factor is that of an infinitely thin rod of length, L,

$$P_L(Q) = L^2\left[\frac{2Si(QL)}{QL} - \frac{4\sin^2(QL/2)}{(QL)^2}\right],$$

where $Si(x) = \int_0^x t^{-1}\sin t\,\mathrm{d}t$. The cross-sectional form factor is,

$$P_{CS}(Q) = \Delta\rho^2\pi R^2\left(\frac{2J_1(QR)}{QR}\right)^2,$$

where R is the cross-sectional radius and J_1 is a first-order Bessel function. [23] Such a function can be used to track the transformation from spherical to worm-like micelles, for example the worm-like micelles which form when mixing of 2 mol dm^{-3} sodium chloride (NaCl) solution with a sodium dodecylsulfate (SDS) micellar solution. This is shown in Figure 6, where time-dependent SAXS (TD-SAXS) was used to observe this transition. [24] TD-SAXS was used to measure the rate at which the SDS micelle changed shape from spherical to worm-like upon the addition of the salt solution. By fitting the data using functions like those discussed it was possible to show that under high salt conditions the micelles transitioned from globular to worm-like in just 200 ms.

2.3. Structure factor

The structure factor is the scattering interference that arises from the interaction of different particles, it is related to the pair distribution function of the particles in solution. [25] The structure factor is the concentration dependent factor within the scattering pattern, and therefore a concentration series can be used to differentiate the scattering from each of the form and the structure factors. It is also possible for addition of salt to affect the presence of the structure factor, for example polyelectrolytes will have their charge screened by the presence of salt, decreasing electrostatic interactions, hence decreasing the apparent structure factor. Similar to the form factor, a large library of existing solutions for the structure factor under different conditions have been generated. These are calculated from liquid state integral equation theory, [26] where the structure factor has the following relation,

$$S(Q) = \frac{1}{1 - Dc(r)},$$

where, D is the number density of the particles and $c(r)$ is the closure relation that allows the solution of the Ornstein-Zernike equation.

Systems of non-ionic micelles lack charged head groups and therefore have no repulsive interactions. This allows the structure factor to be modelled with a hard-sphere, within the Percus-Yevick approximation (PY). [27]

$$c(r) = g(r)\left[\exp\left(\frac{v(r)}{k_B T}\right) - 1\right],$$

where $g(r)$ is the radial distribution function of the particles, $v(r)$ is the potential energy between the particles at distance r, k_B is the Boltzmann constant, and T the absolute temperature. This closure is also applicable to the sticky hard-spheres, where there is an attraction between particles

when the particles are close together. If the micelles are charged, it is necessary to consider a screened Coulombic repulsion between the micelles. This can be achieved at high densities through the mean-spherical approximation (MSA), [28]

$$c(r) = \frac{-v(r)}{k_B T}.$$

Figure 7 shows a comparison between the potential energy, $v(r)$, for each of the three structure factors discussed above.

In addition to simple shape modeling for small angle scattering, scattering patterns for complex, atomistic models of molecules, such as proteins in solution, can be calculated, and fitted to experimental data using programs such as SASSIE [29] or the program suite ATSAS [30]. Since such large, flexible molecules exhibit a range of conformations in solution, the fitting results from these methods generally provide an array of potential, probable conformations that contribute to the observed scattering signals, rather than a single solution structure.

3. APPLICATIONS

It is important to consider how the model-dependent determination of both the form and structure factor is applied in practice. Here we shall give a flavour of the application of this model-dependent approach as it is applied in a series of scientific examples; from a series of areas related to supramolecular organic chemistry.

3.1. Small molecule surfactants

Due to the hydrophobic nature of carbon nanotubes (CNTs) it is necessary to utilise the sequestration behavior of surfactant molecules in order to disperse the CNTs in solution, most commonly used are sodium dodecylsulfate (SDS) and sodium cholate. Kastrisinaki-Guyton and co-workers [31] used combined SANS and SAXS to show that the SDS molecules are not successful in sequestering individual single walled CNTs, rather the CNTs would form small bundles around which surfactants assemble. Different contrasts were used, including one where the proportion of the hydrogenated and deuterated surfactant was such that it was contrast matched to the solvent in order to only give scattering from the CNTs (Figure 8b). The SAS patterns were fitted with a core-shell cylinder model, similar to that discussed earlier. Using this it was possible to show that the system consisted of CNT-cores with a radius of (20 ± 14) Å, with an 18 Å SDS corona, and 50 % volume fraction. If the SDS were to completely cover the surface of each CNT a core-radius of 10 Å and 100 % volume fraction would be expected.

The use of structure-factor based modelling allowed Das and co-workers [32] to show that the size of a CTAB/NaSaI (sodium salicylate) micelle varied inversely with temperature. In this work the SANS form factor was fitted with a polydisperse worm-like chain, using the methods mentioned previously, with the worm-radii and worm-lengths being integrated over a range. The structure factor evaluation involved the use of the random phase approximation.

$$S(Q) = \frac{1}{1 + \beta P_L(Q, L)},$$

where, $P_L(Q, L)$ is the longitudinal form factor, which varies with worm-length (L) and β varies with the forward scattering contribution to the structure factor, $S(0)$,

$$\beta = \frac{[1 - S(0)]}{S(0)}.$$

The forward scattering contribution to the structure factor is dependent on the volume fraction of the micelles, indicating the concentration dependence. Using this model-dependent analysis method it was possible to show Arrhenius behavior of the micelle worm-length (Figure 9) with temperature.

Recent work which has combined the use of model-dependent analysis with the methods of Glatter and co-workers [14] for a combined SANS/SAXS study, is that of Sanchez-Fernandez and co-workers. [33] This work used inverse Fourier transform techniques to suggest the presence of cylindrical micelles of sodium dodecylsulfate (SDS) in the deep eutectic solvent (DES) choline chloride/urea compared to the spherical micelles observed in aqueous solution. Further analysis was not possible using these techniques the due to the structure factor present in the scattering pattern. Model-dependent analysis was then used to evaluate the patterns including the extent of interactions between micelles, and to further parameterize the size and shape of these micelles, including determining the choline chloride component of the DES to be in closer proximity to the micelle interface than the urea. Further the model dependent analysis was able to show that the addition of water to the system, or increase of the surfactant concentration, decreased the length of the cylindrical micelles (Figure 10).

3.2. Polymers

Polymeric systems offer an interesting area of study due to the influence of their highly fractal nature on the form factor modelling. Jaksch and co-workers [34] investigated the thermo-responsivity of poly(*iso*-propyl-2-oxazoline)s (P*i*PrOx) gradient polymers using time-resolved SANS. The scattering from the single polymer chains and small aggregates was modelled using a form factor for small, fractal objects, which is dependent on the overall size of the chain, ξ. Two different temperature jumps were used which passed through the polymer cloud point, a shallow and a deep quench which correspond to temperature changes from 25 °C to 27 °C and 25 °C to 30 °C respectively. It was noted that the chain size for the single chains and small aggregates dropped significantly more in the deep quench system compared to the shallow. This is indicative of a more pronounced collapse during the deep quench temperature jump.

The probing nature of SANS also allowed for the determination of the internal structure of polymeric nanoparticles in the work of Yang and co-workers. [35] This

work used SANS to explain the difference in drug loading and release from poly(lactide-*co*-glycolide)-*block*-poly(ethylene glycol) (PLGA-PEG-CH_3) particles. This showed that the nanoparticles consisted of 7-9 nm PLGA blocks encapsulated within a fractal PEG/water network. The use of model-dependent analysis allowed for the parameterization of the PLGA block radius, fractal dimension, and correlation length. This analysis revealed that the water miscibility of the solvent used in the nanoparticle synthesis had an effect on the resulting structure, with those prepared using solvents with greater water miscibility resulting in smaller PLGA block structures.

The development of polymeric materials for drug delivery has been investigated heavily in recent years, particularly with SAS. Zhang and co-workers [36] used SANS to study the aqueous structure of the boronic acid-functionalised block co-polymer, PEG-b-PPBDEMA, where the PEG content was 24 wt%. Form factor based analysis was capable of showing an interesting morphological response to the addition of glucose solution. The polymers initially had a vesicular form, which could be fitted with a spherical core shell model. Following the addition of glucose, these vesicles contracted due to the higher external osmotic pressure compared to that of the aqueous interior. However, the glucose could react reversibly with the PBDEMA blocks increasing the hydrophilic-to-hydrophobic volume ratio and causing the size and volume of the vesicle to increase above that initially held (1.55×10^8 Å^3 to 2.07×10^8 Å^3). Increasing the pH of the solution by the addition of NaOD increased further the ionization of the PBDEMA blocks and hence the hydrophilic-to-hydrophobic volume ratio causing further change in the structure from vesicular to cylindrical aggregates. This glucose based structural transformation could be used as the basis for future work on the development of glucose responsive insulin encapsulation and release for the treatment of diabetes.

3.3. Peptides

SAS has also been applied to the study of biologically relevant self-assembling systems such as the peptide series A_nK, where A is the amino acid alanine, K is lysine, and *n* is 4-10. [37] SAXS was used to show that the A_4K was highly soluble at the concentration investigated with no scattering present. A_6K had previously been observed to form hollow nanotubes with a cross section of 52 nm and a nematic liquid crystalline phase behavior. A_8K and $A_{10}K$ showed different self-assembly behavior to that observed for A_6K. [38, 39] For these peptides with a greater number of alanine amino acids, rod-like structures were observed with cryoTEM. However, the longitudinal dimension could not be quantified with SAXS, as it was out with the Q-range of the instrument used ($0.1\ \text{nm}^{-1} \leq Q \leq 4\ \text{nm}^{-1}$, i.e. rod-length > 60 nm). The radial structure could however be parameteried with a biaxial cross-section, so the rods had an elliptical cross-section with semiaxes of $a = 1.9$ nm and $b = 4.2$ nm.

The enzymatic breakdown of the peptide amphiphile C_{16}-KKFFVLK by α-chymotrypsin, was shown to result in a change in the self-assembly mechanism by Dehsorki and co-workers. [40] The uncleaved peptide was capable of forming nanotubes and helical ribbons with a significant amount of β-sheet character. However, following cleavage, which occurs at either the phenylalanine-phenylalanine (F-F) bond of the phenylalanine-valine (F-V) bond, the β-sheet character is almost completely lost. SAXS was able to identify the formation of spherical micelles in the solution of the disrupted structure, which were shown to belong to the C_{16}-KKF or the C_{16}-KKFF, which were isolated by mass spectroscopy. By the fitting of a spherical form factor it was possible to show that the micelles had a diameter of ~5 nm (Figure 11).

4. CONCLUSIONS

We have introduced the importance and applicability of small-angle scattering in the analysis of complex organic supramolecular structures. The theory behind the use of small-angle scattering was introduced and discussion of some common analytical methods followed. These only offer an introduction to the depth of analysis which is available when using small-angle scattering. Not covered were areas of ab-initio modelling, such as DAMMIF [41] or SASSIE, [29,42] where near-atomistic structural models can be developed for high quality data. Finally, some possible applications of this model-dependent analysis techniques were covered, from three areas of organics chemistry; small molecule surfactants, polymeric systems, and peptide self-assembly.

CONFLICT OF INTEREST

The authors declare no competing financial interest.

ACKNOWLEDGEMENTS

ARM would like to thank the University of Bath and Diamond Light Source for co-funding a PhD studentship (Diamond studentship number STU0149).

REFERENCES

[1] Philp, D.; Stoddart, J. F.; Self-Assembly in Natural and Unnatural Systems. *Angew. Chem. Int. Ed.,* **1996**, 35, 1154-1196

[2] van Esch, J. H.; Schoonbeek, F.; de Loos, M.; Kooijman, H.; Spek, A. L.; Kellogg, R. M.; Feringa, B. L.; Cyclic Bis-Urea Compounds as Gelators for Organic Sovlents. *Chem. Eur. J.,* **1999**, 5, 937-950

[3] Mohr, B.; Sauvage, J.-P.; Grubbs, R. H.; Weck, M.; High Yield Synthesis of [2] Catenanes by Intermolecular Ring-Closing Metathesis. *Angew. Chem. Int. Ed*., **1997**, 36, 1308-1310

[4] Hammounda, B.; Probing Nanoscale Structure – The SANS Toolbox, http://www.ncnr.nist.gov/staff/hammouda/the_SANS_toolbox.pdf (Accessed Oct 28, **2016**)

[5] Feigin, L. A.; Svergun, D. I.; Structure Analysis by Small-Angle X-ray and Neutron Scattering; Plemun Press: New York & London, **1987**

[6] Glatter, O.; Kratky, O.; Small Angle Scattering; Academic Press; London, **1982**

[7] SASview for Small Angle Scattering. http://www.sasview.org/ (Accessed Oct 26, **2016**).

[8] Breßler, I.; Kohlbrecher, J.; and Thünemann, A. F.; SASfit: a tool for small-angle scattering data analysis using a library of analytical expressions. *J. Appl. Crystallogr.*, **2015**, 48, 1587-1598

[9] Pernot, P.; Round, A.; Barrett, R.; Antolinos, A. D. M.; Gobbo, A.; Gordon, E.; Huet, J.; Kieffer, J.; Lentini, M.; Mattenet, M.; Morawe, C.; Mueller-Dieckmann, C.; Ohlsson, S.; Schmid, W.; Surr, J.; Theveneau, P.; Zerrad, L.; McSweeney, S.; Upgraded

ESRF BM29 beamline for SAXS on macromolecules in solution. *J. Synchrotron Radiat.,* **2013**, 20, 660-664
[10] Stribeck, N. X-ray Scattering of Soft Matter; Springer: Berlin, **2007**
[11] Schurtenberger, P. In: *Neutrons, X-rays, and Light: Scattering Methods Applied to Soft Condensed Matter*; Linder, P and Zemb T., Ed.; Elsevier Science B. V: Amsterdam, **2002**; pp. 145-170.
[12] Edler, K. J.; Bowron, D. T. Combining wide-angle and small-angle scattering to study colloids and self-assembly. *Curr. Opin. Colloid Interface Sci.*, **2015**, 20, 227-234
[13] Conrad, H.; Dose, K.; Nawroth, T.; Neutron small angle scattering of micelles from detergents suitable for the solubilization of native membrane proteins. *Physica B: Condens. Matter*, **1989**, 156 & 157, 474-476
[14] Glatter, O. In: *Neutrons, X-rays, and Light: Scattering Methods Applied to Soft Condensed Matter*; Linder, P and Zemb T., Ed.; Elsevier Science B. V: Amsterdam, **2002**; pp. 73-102.
[15] Guinier A.; Hebd, C. R.; *Séance Acad. Sci.*, **1937**, 204, 1115
[16] Sivia, D.S. *Elementary Scattering Theory: For X-ray and Neutron Users*; Oxford University Press: Oxford, **2011**.
[17] Skou S.; Gillilan, R. E.; Ando, N.; Synchrotron-based small-angle X-ray scattering of proteins in solution. *Nat. Protoc.,* **2014**, 9, 1729-1739
[18] Porod G.; *Kolloid Zeitschrift*, **1951**, 124, 83
[19] Pedersen J. S.; Analysis of small-angle scattering data from colloids and polymer solutions: modeling and least-squares fitting. *Adv. Colloid Interface Sci.,* **1997**, 70, 171-210
[20] Pedersen, J. S. In: *Neutrons, X-rays, and Light: Scattering Methods Applied to Soft Condensed Matter*; Linder, P and Zemb T., Ed.; Elsevier Science B. V: Amsterdam, **2002**; pp. 391-420.
[21] Brennan, T.; Roser, S. J.; Mann, S.; Edler, K. J.; The Structural Evolution of Surfactant Silica Film Forming Solutions, Investigated Using Small Angle Neutron Scattering. *Chem. Mater.* **2002,** 14, 4292-4299
[22] Porte, G.; Poggi, Y.; Appell, J.; Maret, G.; Large micelles in concentrated solutions. The second critical micellar concentration. *J. Phys. Chem.*, **1984**, 88, 5713-5720
[23] Pedersen, J. S. In: *Soft-Matter Characterization*; Borsoli, R and Pecora R., Ed.; Springer: New York, **2008**; pp. 191-233
[24] Jensen, G. V.; Lund, R.; Gummel, J.; Narayanan, T.; Pedersen, J.S.; Monitoring the Transition from Spherical to Polymer-like Surfactant Micelles Using Small-Angle X-Ray Scattering. *Angew Chem. Int. Ed.*, **2014**, 53, 11524–11528
[25] Klein, R. In: *Neutrons, X-rays, and Light: Scattering Methods Applied to Soft Condensed Matter*; Linder, P and Zemb T., Ed.; Elsevier Science B. V: Amsterdam, **2002**; pp. 351-380.
[26] Hansen, J.P.; McDonald, I. R.; *Theory of Simple Liquids*; Academic Press: San Diego, **1986**.
[27] Vrij, A; Mixtures of hard spheres in the Percus-Yevick approximation. Light scattering at finite angles. *J. Chem. Phys.*, **1979**, 71, 3267-3270
[28] Ruiz-Estrada, H.; Medina-Noyola, M.; Nägele, G.; Rescaled Mean Spherical Approximation for Colloidal Mixtures. *Physica A*, **1990**, 168, 919-941
[29] Perkins, S. J.; Wright, D. W.; Zhang, H.; Brookes, E. H.; Chen, J.; Irving, T. C.; Krueger, S.; Barlow, D. J.; Edler, K. J.; Scott, D. J.; Terrill, N. J.; King, S. M.; Butler, P. D.; Curtis, J. E., Atomistic modelling of scattering data in the Collaborative Computational Project for Small Angle Scattering (CCP-SAS) *J. Appl. Crystallogr.* **2016,** 49, 1861-1875.
[30] Petoukhov, M. V.; Franke, D.; Shkumatov, A. V.; Tria, G.; Kikhney, A. G.; Gajda, M.; Gorba, C.; Mertens, H. D. T.; Konarev, P. V.; Svergun, D. I., New developments in the ATSAS program package for small-angle scattering data analysis. *J. Appl. Crystallogr.* **2012,** 45, 342-350.
[31] Kastrisianaki-Guyton, E. S.; Chen, L.; Rodgers, S. E.; Cosgrove, T.; van Duijneveldt, J. S.; Adsorption of sodium dodecylsulfate on single-walled carbon nanotubes characterised using small-angle neutron scattering. *J. Colloid Interface Sci.,* **2016**, 472, 1-7
[32] Das, N. C.; Cao, H.; Kaiser, H.; Warren, G. T.; Shape and size of highly concentrated micelles in CTAB/NaSal solutions by small angle neutron scattering (SANS). *Langmuir,* **2012**, 28, 11963-11968
[33] Sanchez-Fernandez, A.; Edler, K. J.; Arnold, T.; Heenan, R. K.; Porcar, L.; Terrill, N. J.; Terry, A. E.; Jackson, A. J.; Micelle structure in a deep eutectic solvent: a small-angle scattering study. *Phys. Chem. Chem. Phys.,* **2016**, 18, 14063-14073
[34] Jaksch, S.; Schulz, A.; Kyriakos, K.; Zhang, J.; Grillo, I.; Pipich, V.; Jordan, R.; Papadakis, C. M.; The collapse and aggregation of thermoresponsive poly(2-oxazoline) gradient copolymers; a time-resolved SANS study. *Colloid. Polym. Sci.,* **2014**, 292, 2413-2425
[35] Yang, B.; Lowe, J. P.; Schweins, R.; Edler, K. J.; Small Angle Neutron Scattering Studies on the Internal Structure of Poly(lactide-*co*-glycolide)-*block*-poly(ethylene glycol) Nanoparticles as Drug Delivery Vehicles. *Biomacromolecules*, **2015**, 16, 457-464
[36] Zhang, Y.; Zhao, W.; Yang, J.; Hammouda, B.; Yang, J.; Cheng, G.; SANS study on self–assembled structures of glucose-responsive phenylboronate ester- containing diblock copolymer; a time-resolved SANS study. *Eur. Polym. J.,* **2016**, 83, 173-180
[37] Cenker, Ç. Ç.; Bucak, S.; Olsson, U.; Aqueous self-assembly within the homologous peptide series A_nK. *Langmuir.,* **2014**, 30, 10072-10079
[38] Bucak, S.; Cenker, Ç. Ç.; Nasir, I.; Olsson, U.; Peptide Nanotube Nematic Phase. *Langmuir.,* **2009**, 25, 4262-4265
[39] Cenker, Ç. Ç.; Bucak, S.; Olsson, U.; Nanotubes and bilyaers in a model peptide system. *Soft Matter.,* **2011**, 7, 4868-4875
[40] Dehsorkhi, A.; Hamley, I. W.; Seitsonsen, J.; Ruokolainen, J.; Tuning Self-Assembled Nanostructures Through Enzymatic Degradation of a Peptide Amphiphile. *Langmuir.,* **2013**, 29, 6665-6672
[41] Franke, D.; Svergun, D. I.; DAMMIF, a program for rapid ab-initio shape determination in small-angle scattering. *J. Appl. Crystallogr.,* **2009**, 42, 342-346
[42] Watson, M.; Curtis, J.; Rapid and accurate calculation of small-angle scattering profiles using the golden ratio. *J. Appl. Crystallogr.,* **2013**, 46, 1171-1177

Figures

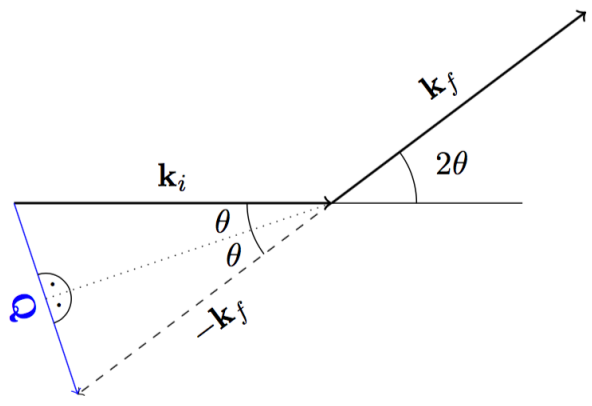

Figure 1. A vector diagram describing an elastic scattering event.

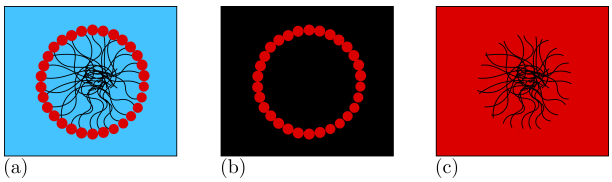

Figure 2. The power of contrast variation for a micelle system, where (a) is the system in pure solvent, while (b) has the solvent scattering matched to the surfactant tails, and (c) has the solvent matched to the surfactant heads.

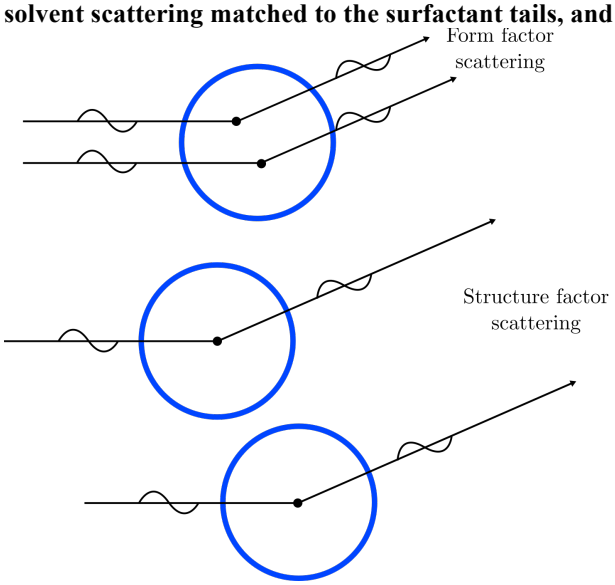

Figure 3. The form factor arises due to the scattering from different parts of the same particle, whereas the structure factor is an inter-particle scattering function.

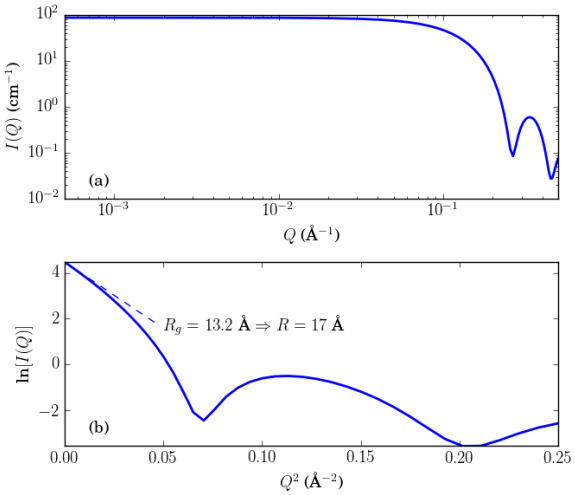

Figure 4. The Guinier approximation, (a) shows the curve from decyltrimethylammonium bromide micelles, generated with SASView [7]. While (b) gives the associated Guinier plot, with the dotted line at low-Q showing the radius of gyration, R_g.

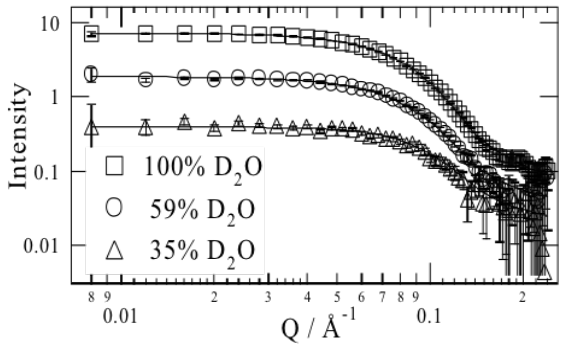

Figure 5. The SAS profile of a hexadecyltrimethylammonium bromide micelle in methanol/water mixtures fitted with a model for ellipsoids. Reprinted with permission from Ref. [21]. Copyright 2002 American Chemical Society.

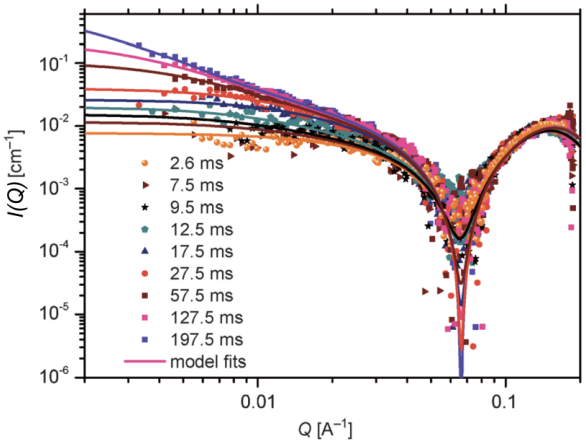

Figure 6. Time-dependent SAXS from stopped-flow apparatus. Data obtained after mixing of SDS (1 %) with 2 mol dm^{-3} NaCl solution. Solid lines correspond to data fitted with a worm-like core-shell model. Reproduced with permisssion from Ref. [24] © 2014 WILEY-VCH Verlag GmbH & Co. KGaA, Weinheim.

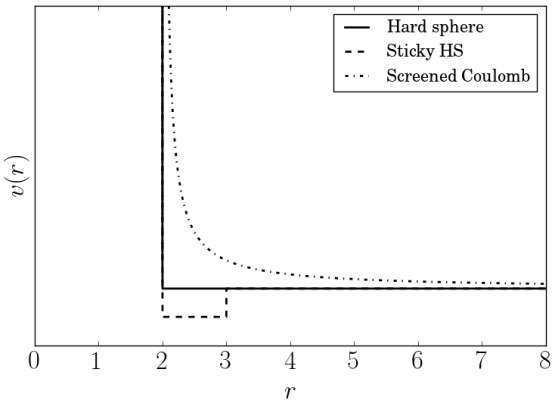

Figure 7. The potential energy functions for each of the structure factors discussed here.

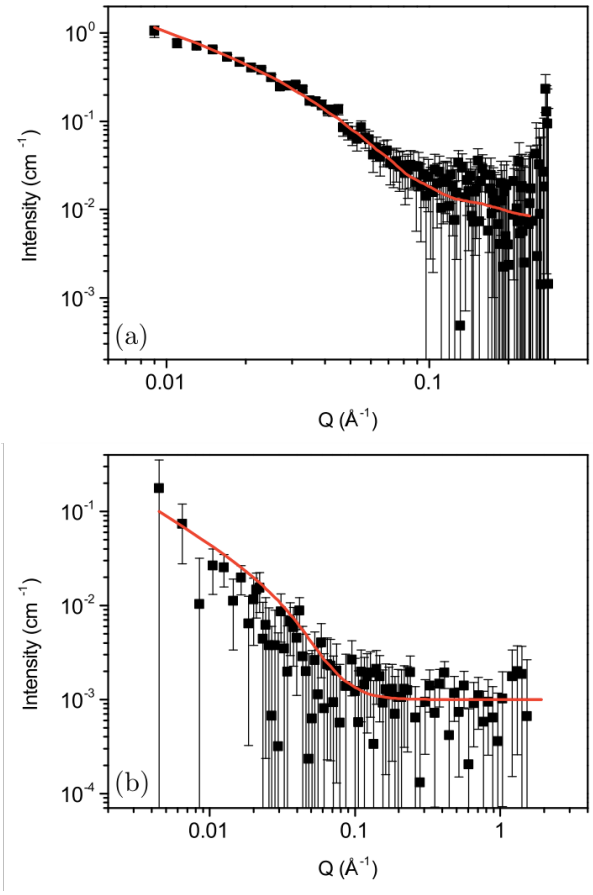

Figure 8. The fitted SANS of (a) h-SDS in D_2O with SWCNTs, and (b) contrast matched-SDS in D_2O with SWCNTs, from Ref. [29] under a Creative Commons Attribution License (CC BY).

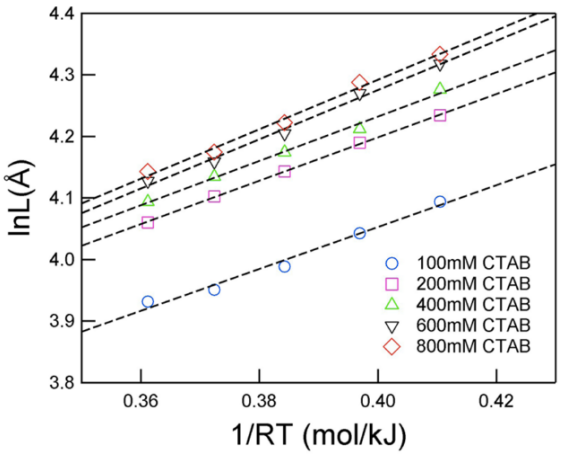

Figure 9. The micelle worm-length as a function of temperature, demonstrating Arrhenius-like behavior. Reprinted with permission from Ref. [30]. Copyright 2012 American Chemical Society.

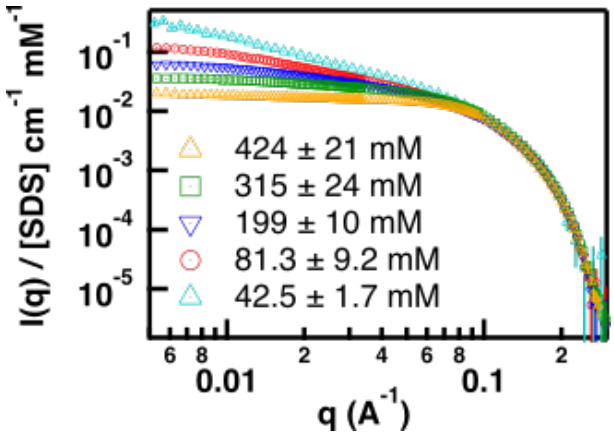

Figure 10. The fitted SAS profiles, showing the effect of increasing the surfactant concentration on the shape of the SDS micelles, from Ref. [31] -- Published by the Royal Society of Chemistry usage under the Creative Commons Attribution 3.0 Unported License.

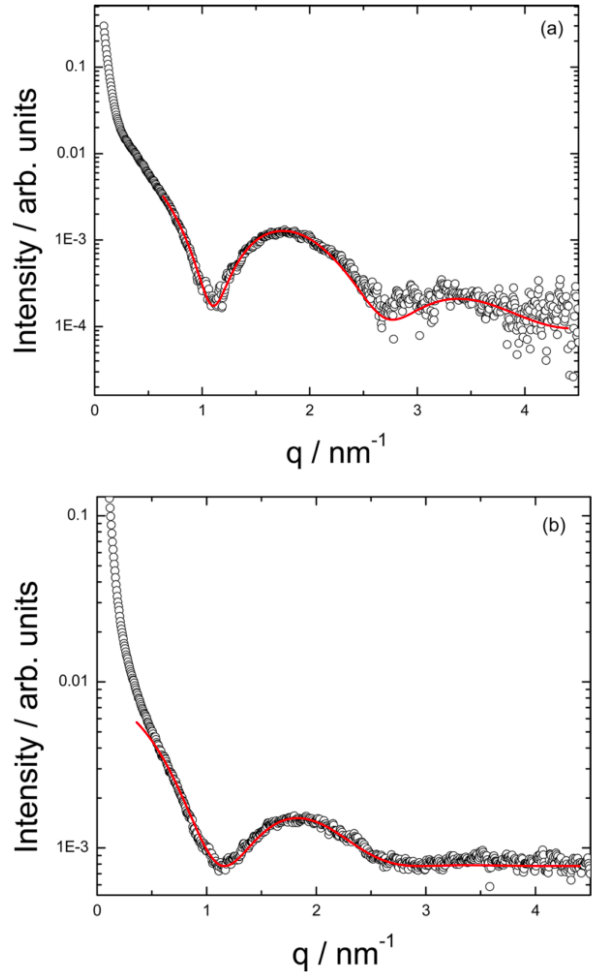

Figure 11. The SAXS profiles fitted with a spherical form factor for (a) 0.5 wt% C_{16}-KKF and (b) 0.5 wt% C_{16}-KKFF, from Ref. [38] usage under the Creative Commons Attribution 4.0 License.